

Measurements of bicoherence and long-range correlations during biasing in the HSX stellarator

This content has been downloaded from IOPscience. Please scroll down to see the full text.

2011 Nucl. Fusion 51 083048

(<http://iopscience.iop.org/0029-5515/51/8/083048>)

View [the table of contents for this issue](#), or go to the [journal homepage](#) for more

Download details:

IP Address: 128.104.46.196

This content was downloaded on 10/03/2016 at 20:39

Please note that [terms and conditions apply](#).

Measurements of bicoherence and long-range correlations during biasing in the HSX stellarator

R.S. Wilcox¹, B.Ph. van Milligen², C. Hidalgo², D.T. Anderson¹, J.N. Talmadge¹, F.S.B. Anderson¹ and M. Ramisch³

¹ Department of Electrical and Computer Engineering, University of Wisconsin–Madison, Madison, WI 53706, USA

² Asociación EURATOM-CIEMAT, Avda. Complutense 22, 28040 Madrid, Spain

³ Institut für Plasmaforschung, Universität Stuttgart, D-70569 Stuttgart, Germany

Received 13 January 2011, accepted for publication 4 July 2011

Published 29 July 2011

Online at stacks.iop.org/NF/51/083048

Abstract

The effect of biasing on edge fluctuations has been studied in the HSX stellarator using Langmuir probes. Biasing leads to an increase in the bicoherence of the poloidal electric field, as well as a simultaneous increase in long-range correlations of the floating potential, measured using toroidally separated Langmuir probes. These observations are consistent with zonal flow formation. A comparison has been made between experiments in an optimized quasi-symmetric magnetic configuration (quasi-helically symmetric—QHS) and a configuration with the symmetry intentionally degraded (mirror). The observed differences are insignificant and most likely unrelated to the change in configuration.

(Some figures in this article are in colour only in the electronic version)

1. Introduction

In spite of considerable efforts, the physical mechanism of spontaneous L–H confinement transitions in fusion plasmas is still not understood in full detail. One model finds that the sheared poloidal flows leading to these confinement transitions are the consequence of the non-linear energy transfer between broadband drift wave turbulence and low- k zonal flows [1]. This energy transfer from the turbulence towards low mode number poloidal flows via the Reynolds stress leads to a reduction in turbulent transport and a subsequent increase in the ion pressure gradient. This gradient increases the radial electric field shear, which further reduces transport, and a large equilibrium $E \times B$ flow shear can be sustained. At this point, turbulence is no longer available to drive the zonal flows, but the equilibrium flow shear remains, radial transport is reduced and a pedestal is created in the plasma pressure profile [1–3]. While this theory explains many phenomena observed in experiments, further characterization of confinement transitions is necessary for the design of future devices. Here we examine the effect of mean radial electric fields on zonal flows, as well as the effect that the magnetic configuration has on zonal flow formation.

Bicoherence analysis is capable of detecting non-linear three-wave coupling, and so it is expected to be a useful tool for understanding zonal flow formation and confinement

transitions [3–5]. Indeed, enhanced levels of bicoherence of the density, potential or velocity signals have been correlated with the triggering of sheared flows during spontaneous L–H transitions in tokamaks and stellarators [3–7]. Enhanced levels of bicoherence in these signals have also been measured during bias-induced confinement transitions in the devices CCT [5] and TJ-II [7], which suggest a common mechanism between forced and spontaneous confinement transitions.

The effect of neoclassical optimization on anomalous transport and zonal flows in stellarators has been studied at LHD, where reduced anomalous transport was measured in the ‘inward shifted’ configuration designed to reduce neoclassical transport. This anomalous transport reduction has been attributed to higher levels of zonal flows [8]. The optimization of helical configurations with the purpose of reducing neoclassical transport has been predicted to lead to a concomitant reduction in anomalous transport by enhancing the zonal flow response [9, 10]. This situation would of course be very attractive, as both neoclassical and anomalous transport could be reduced simultaneously.

This work reports on measurements of the bicoherence at the Helically Symmetric Experiment (HSX), a stellarator optimized for quasi-helical symmetry. In this case, the magnetic field strength possesses a helical direction of symmetry, similar to the toroidal direction of symmetry in a tokamak [11, 12]. This optimization has been shown to reduce

the neoclassical transport [13] as well as the neoclassical flow damping in the direction of symmetry [14]. Here we measure the bicoherence in two magnetic configurations at HSX: one with the quasi-helical symmetry optimized and one in which this symmetry has been intentionally degraded. In this paper, we will test whether the degree of symmetry affects the formation of zonal flows and the detection of bicoherence.

The presence of zonal flows can be detected independently by measuring the long-range correlations of plasma potential fluctuations using toroidally separated Langmuir probes, as shown in the stellarators TJ-II [15] and TJ-K [16], as well as the TEXTOR tokamak [17]. In this work, we report on similar measurements at HSX, using multiple Langmuir probes placed around the device.

2. Experimental setup

HSX plasmas studied here have an on-axis magnetic field strength of 1 T and 50 kW of injected power, using fundamental ordinary mode electron cyclotron resonance heating (ECRH) at 28 GHz. The rotational transform has low shear across the plasma radius, going from $\iota(0) = 1.05$ in the core to $\iota(a) = 1.12$ at the edge. Electron densities in the edge region (at the position of the probes) are approximately $1 \times 10^{18} \text{ m}^{-3}$ and hydrogen is used as the working gas. The stainless-steel walls were conditioned with boron prior to these experiments, which led to greater density control and lower radiated power relative to the previous carbon conditioning.

The optimized magnetic configuration in HSX is designed to be quasi-helically symmetric (QHS configuration). Planar auxiliary coils can be energized to break this symmetry by adding additional terms to the magnetic spectrum. The denoted ‘mirror’ configuration is a specific magnetic configuration that breaks the symmetry with minimal changes in other parameters such as the mean field strength, well depth and rotational transform [18]. This configuration allows a comparison of plasmas with quasi-symmetry versus plasmas with the symmetry broken, and has been used for the comparisons presented here.

One measure of the neoclassical optimization of the magnetic field is the effective ripple, ε_{eff} . This quantifies the unfavourable $1/\nu$ transport that is exhibited in non-symmetric magnetic configurations, including rippled tokamaks, at low collisionality [19]. The $1/\nu$ transport scales with $\varepsilon_{\text{eff}}^{3/2}$ for zero radial electric field in the low collisionality regime. In the edge region where probe measurements can be taken, the effective ripple in the QHS configuration is approximately 1×10^{-2} , and $\sim 5 \times 10^{-2}$ in the mirror configuration (figure 2 [18]). The difference in the degree of symmetry breaking between the two configurations at the edge is not as great as it is further into the plasma, where the QHS configuration is better optimized. By comparison, NSTX with RMP coils has an ε_{eff} of $\sim 10^{-3}$ at the edge [20], and the conventional stellarator TJ-II at the edge has an ε_{eff} of ~ 0.5 [21].

A 5-pin Langmuir probe is installed on HSX, a diagram of which is presented in figure 1. Three pins (pins 2, 3 and 4) are aligned poloidally on a toroidal cut of the same flux surface. The centre pin (pin 3) is biased to measure ion saturation current while the end pins (2 and 4) measure the

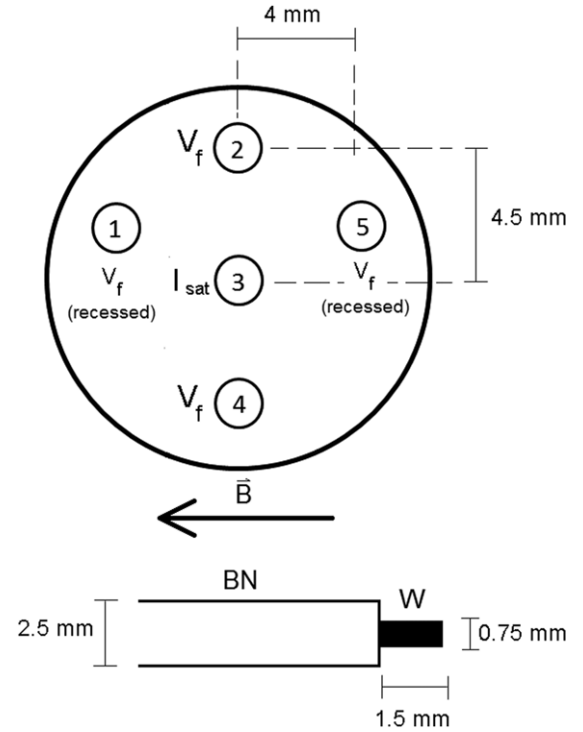


Figure 1. Probe tip configuration for fluctuation measurements. Tungsten tips shielded with boron nitride tubes extend 2 cm out from the bulk boron nitride shell. Pins 1 and 5 are recessed 4 mm radially.

floating potential. Using this configuration, the instantaneous poloidal electric field can be inferred from

$$E_{\theta} = \frac{V_{f,4} - V_{f,2}}{|x_4 - x_2|}, \quad (1)$$

where $V_{f,4}$ and $V_{f,2}$ are the floating potentials measured at pins 4 and 2, respectively, and $|x_4 - x_2|$ is the linear distance between the two pins in the poloidal plane. While electron temperature fluctuations may in principle affect this measurement, it has been shown that the fluctuating floating potential measured with Langmuir probes is in fact a good proxy for the fluctuating plasma potential in the relevant plasma conditions [22], and so we will ignore the contribution of temperature fluctuations here. The final two pins, pins 1 and 5, are recessed radially and are configured to measure floating potential to infer the radial electric field.

The probe is located on the low-field, bad curvature side of the machine, near the plasma mid-plane where the flux surfaces are compressed. Figure 2 shows a cross-section of the magnetic surfaces at the probe’s location along with the probe measurement points in the QHS configuration. The surfaces shift slightly when the configuration is changed to mirror, but the shaping remains largely intact. Radial scans of the probe are taken on a shot-by-shot basis. Discharges in HSX are limited to 50 ms of ECRH, about 30 ms of which has a line-averaged density that is constant during the discharge to within 5% and a stored energy that is constant to within the measurement error, $\sim 10\%$.

For the long-range correlation studies, a reference probe with a single pin is used. This probe is placed at $\rho = r/a = 0.9$ and left stationary while the 5-pin probe is scanned radially.

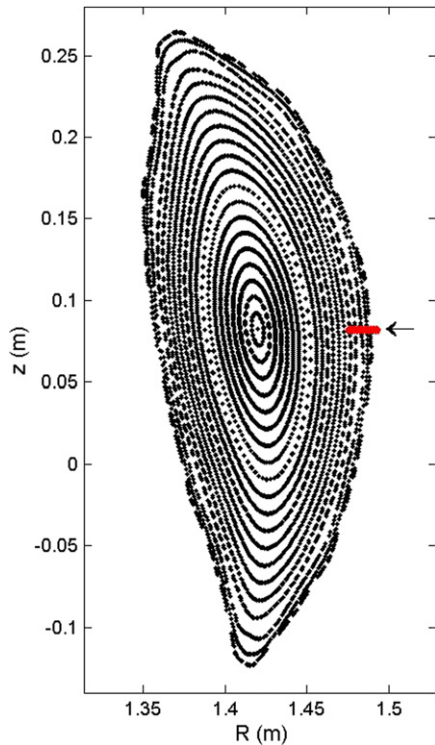


Figure 2. A toroidal cross-section of a QHS plasma at the 5-pin probe location (shown in figure 3). The arrow indicates the position of the probe. The magnetic field is directed primarily into the page, and the radial range of the measurements is indicated in red.

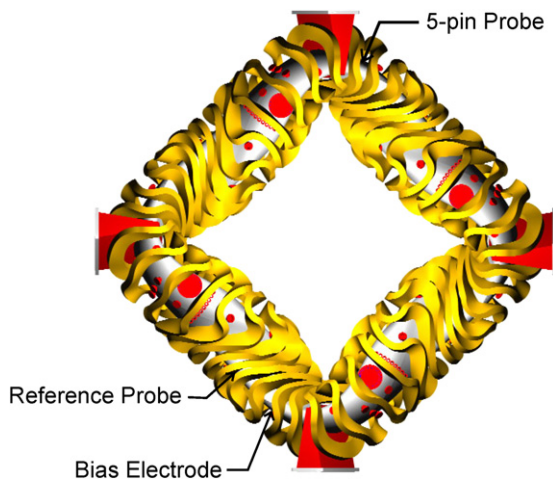


Figure 3. Top view of HSX vessel, coils, and ports. Bicoherence measurements are made using the 5-pin Langmuir probe at top, and the long-range correlation analysis is performed between this probe and the reference probe.

The location of this reference probe on HSX, as well as the placement of the 5-pin probe and the bias electrode, is shown in figure 3.

The HSX bias probe consists of a molybdenum cylinder, 10 mm in diameter, encased in an insulating boron nitride shell. The final 5 mm of the probe are exposed radially to the plasma. A positive bias voltage is applied with respect to both the vessel and a carbon plate placed just outside the last closed flux surface. The carbon plate is located approximately one

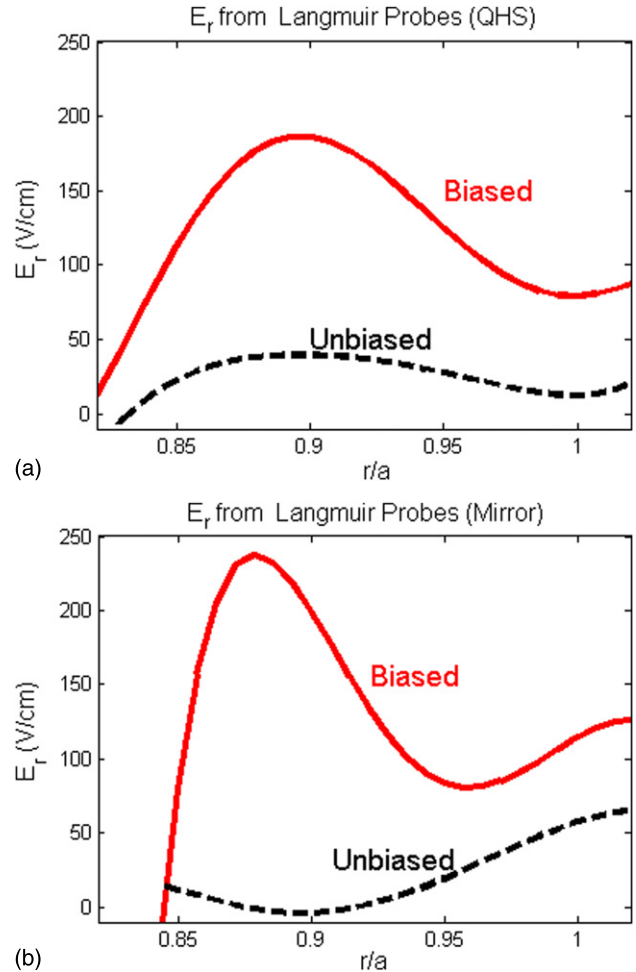


Figure 4. Radial electric field profiles in the (a) QHS and (b) mirror configurations from Langmuir probes. These profiles are calculated by fitting a curve of the shot-by-shot floating potential profile and taking the spatial derivative.

field period away toroidally and 90° poloidally from the bias probe. Measurements show that over 90% of the return current passes through the plate, with the rest going directly to the vessel. This confirms field-line following studies showing that the plate intersects nearly all of the field lines launched from just outside the last closed flux surface.

For these experiments, a positive 250 V bias is applied while the bias probe is located at $\rho \sim 0.75$. The probe draws approximately 18 A of current and imposes a radial electric field as shown in figure 4 for both the QHS and mirror configurations, as measured by Langmuir probes. These values have been calculated by fitting a curve to the shot-by-shot floating potential profile and taking the spatial derivative. Since the electron temperature profile is flat to within the Thomson scattering measurement error in the region of interest in both configurations, the contribution of the electron temperature gradient to V_f is neglected in the calculation of E_r . In the region where $r/a > 0.9$, there are no Thomson scattering measurements, but a temperature gradient may exist that would affect the radial electric field calculation using this method. However, this contribution to E_r will be on the order of $\sim 0\text{--}50 \text{ V cm}^{-1}$, and it will be similar for the biased and unbiased cases, since Thomson

scattering does not show a temperature change in the rest of the edge region during biasing. Without local temperature measurements, this contribution is impossible to localize, and it will thus be ignored. For the discharges analysed here, the bias probe was energized for the final 10 ms of plasma, giving 20 ms of unbiased and 10 ms of biased fluctuation data for each radial location.

An attempt was made to keep turbulent transport drive terms the same between the experiments in the QHS and mirror configurations, so that any difference in measured quantities could be attributed to a change in ε_{eff} . In the QHS and mirror discharges used here, electron density profiles as measured by Thomson scattering match to within the measurement error across the minor radius. Core electron temperatures in the QHS configuration peak at around 1 keV, while those in mirror only reach 600 eV on axis. However at the edge, where these data were taken, both configurations have a negligible temperature gradient and a relatively low electron temperature near 60 eV. The trapped particle fraction is also nearly constant between the two configurations. Due to the small temperature gradients, low electron collisionality and high T_e/T_i , trapped electron mode turbulence is expected to be the dominant transport mechanism in the edge region in HSX [23].

When the bias is applied, the potential profile and radial electric field imposed in both configurations are qualitatively similar, with a large peak in E_r between $\rho = 0.86$ and $\rho = 0.93$, as seen in figure 4. According to Thomson scattering measurements, the temperature profile does not significantly change during biasing in the region measured by the probes. The density gradient in the biased region increases quickly when the bias is applied, and is approximately steady for the time when data presented here are taken.

2.1. Signal processing

The bicorrelation of two signals $X_1(t)$ and $X_2(t)$ with zero mean and unit standard deviation is defined by

$$C_2(t_1, t_2) = \langle X_1(t)X_2(t+t_1)X_2(t+t_2) \rangle, \quad (2)$$

where the angle brackets imply averaging over t . The bispectrum is the Fourier transform of the bicorrelation, and can be written in terms of the Fourier transforms of the signals:

$$B(\omega_1, \omega_2) = \hat{X}_1^*(\omega)\hat{X}_2(\omega_1)\hat{X}_2(\omega_2), \quad (3)$$

where \hat{X} indicates the Fourier transform of X , \hat{X}^* is the complex conjugate of \hat{X} and $\omega = \omega_1 + \omega_2$. The bicoherence is then obtained by averaging the bispectrum over statistically equivalent realizations and normalizing as

$$b^2(\omega_1, \omega_2) = \frac{|\langle B(\omega_1, \omega_2) \rangle|^2}{\langle |\hat{X}_1(\omega)|^2 \rangle \langle |\hat{X}_2(\omega_1)\hat{X}_2(\omega_2)|^2 \rangle}. \quad (4)$$

Here the angle brackets indicate an average over realizations. The normalization is such that $0 \leq b^2 \leq 1$. The bicoherence is symmetric under the transformations $(\omega_1, \omega_2) \rightarrow (\omega_2, \omega_1)$ and $(\omega_1, \omega_2) \rightarrow (-\omega_1, -\omega_2)$, such that only one quarter of the plane (ω_1, ω_2) contains independent information. Additionally, for discretely sampled data all frequencies must be less than the Nyquist frequency: $|\omega_1|,$

$|\omega_2|, |\omega| \leq \omega_{\text{Nyq}}$. These restrictions define a polygonal subspace of the plane, which is how the bicoherence is usually represented, as it is in figure 5. When $X_1 = X_2$, the above quantities are designated auto-bicorrelation, auto-bispectrum and auto-bicoherence, respectively.

The summed bicoherence can also be calculated to reduce the dimensionality of the bicoherence at a given radial location using the expression

$$b_{\text{sum}}^2(\omega) = \frac{1}{N(\omega)} \sum_{\omega_1+\omega_2=\omega} b^2(\omega_1, \omega_2). \quad (5)$$

This quantifies the mean contribution of coupling waves to the mode at the sum frequency.

For the study of the long-range correlations, the coherence is used as an indicator of the spectral similarities of the two fluctuating signals. The coherence presented here is calculated as

$$\gamma(\omega) = \frac{|\langle P_{xy}(\omega) \rangle|}{\sqrt{\langle |P_{xx}(\omega)| \rangle \langle |P_{yy}(\omega)| \rangle}}, \quad (6)$$

where P_{xy} is the cross-spectral density and P_{xx} and P_{yy} are the auto-spectral densities of the fluctuations at the two probe tips and the angle brackets again indicate an average over realizations. The contributions of frequencies below a given level, 10 kHz in this case, are then averaged to give the low-frequency coherence.

3. Results

3.1. Bicoherence

Using these analysis techniques for the HSX Langmuir probe data, it was found that a significant level of broadband auto-bicoherence was measured in the E_θ fluctuations during biasing. The analysis of the auto-bicoherence of E_r signals produced values in the range of the noise, as did the analysis of the cross-bicoherence between E_θ and E_r signals. This situation, while not fully understood, is also encountered at TJ-II [6]. Although density fluctuations were observed to produce significant bicoherence during L–H transitions in DIII-D [24], this was not the case in the biased discharges in HSX.

Figure 5 represents the frequency-resolved auto-bicoherence of the E_θ fluctuations in the (a) QHS and (b) mirror configurations in HSX at multiple radial locations spaced between $\rho = 0.83$ and the last closed flux surface. For each radial position, 20 ms of unbiased and 10 ms of biased fluctuation data are each divided into 200 realizations to be averaged. The colour at a given location in the two-dimensional plot indicates the amount of auto-bicoherence between fluctuations at frequencies f_1 on the x -axis and f_2 on the y -axis, as they correlate with fluctuations of frequency $f_1 + f_2$. Before biasing is applied, the bicoherence at all frequencies is near the noise level, which is 0.005 across all frequencies in these cases, both before and during biasing. When the bias probe is energized, bicoherence significantly higher than the noise level is measured across a broad range of low frequencies in the biased region. The highest peaks in the plots correspond to a bicoherence of 0.12. In both configurations, the region with the highest levels of bicoherence corresponds directly to the region of strongest induced radial electric field.

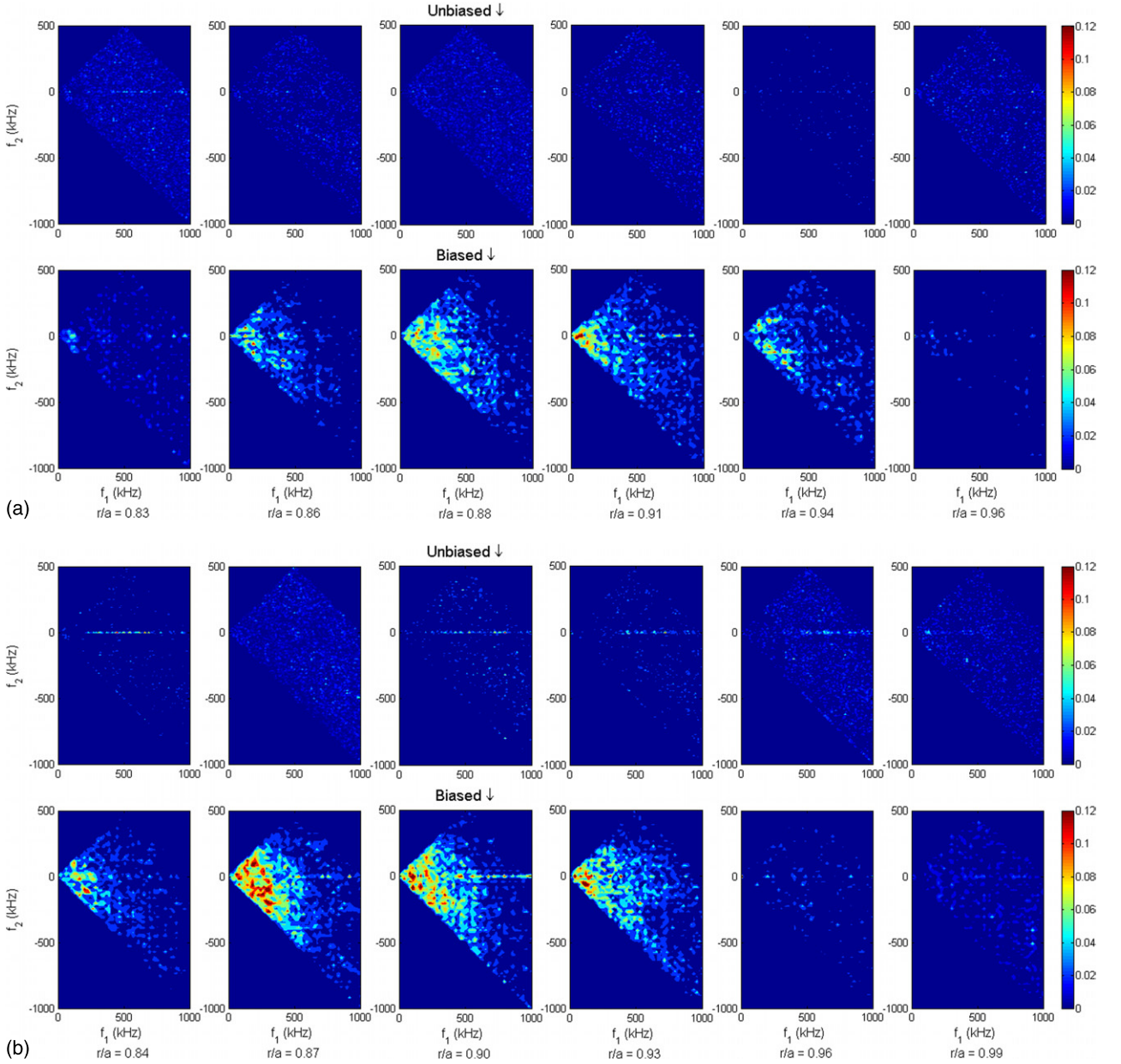


Figure 5. Radial scan of E_θ auto-bicoherence in (a) QHS and (b) mirror configurations. Data from unbiased times are on the top, biased times are at the bottom. In both configurations, broadband coupling is observed in the same region as the large bias-induced radial electric field.

A clear indication of small scale turbulence coupling directly and preferentially to large scale zonal flows would be the appearance of high magnitude bands in this frequency-resolved plot, one at $f_1 \approx f_2$, and the other at $f_2 \approx 0$, as seen in [25]. This is indeed what has been observed in E_θ fluctuations in TJ-II during spontaneous (not biased) transitions to improved confinement regimes [7]. During the biased discharges presented here, broadband coupling is observed in the region of strong induced radial electric field. However, there are no clear indications of direct wave coupling with near-zero frequency zonal flows. This is consistent with previously published measurements of bicoherence in biased discharges of other devices, namely TJ-II [7] and CCT [5]. Although the fluctuations do seem to couple to low frequencies, the latter are not sharply defined. This may

constitute a difference with spontaneous transitions. It should also be noted that the auto-bicoherence of density fluctuations displayed a similar broadband coupling during spontaneous L–H transitions in DIII-D [24].

Figure 6 shows the summed bicoherence of E_θ fluctuations in the QHS (left) and mirror (right) configurations over the full range of measured frequencies. The frequency plotted is f , which includes the summed contributions of all f_1 and f_2 , where $f = f_1 + f_2$. Here it can be seen more clearly that the region with the largest biased radial electric field, roughly $0.86 < \rho < 0.93$ in both configurations, is the same region that measures significant bicoherence while biasing. The location where the largest bicoherence is measured also corresponds to the peak measured E_r in both cases, $\rho = 0.88$ in mirror and $\rho = 0.90$ in QHS. The experiment in the mirror

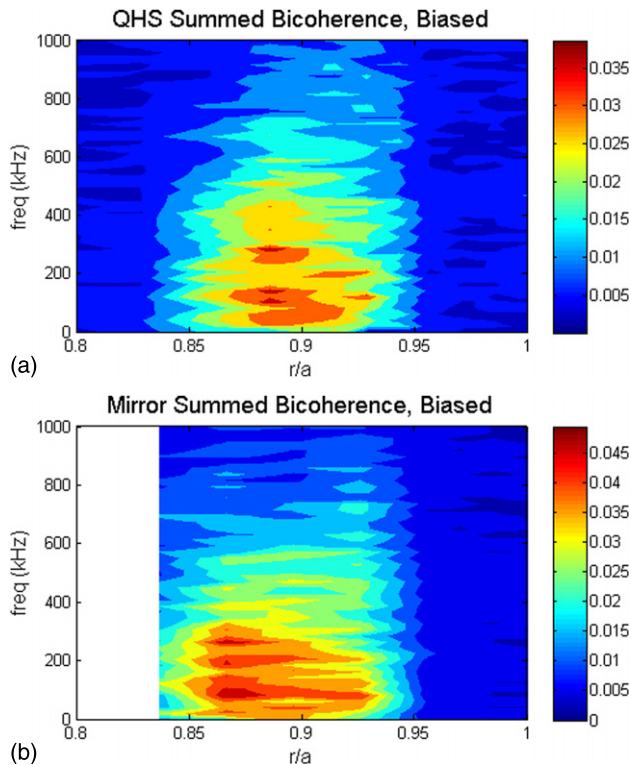


Figure 6. Summed bicoherence as a function of minor radius and frequency during biasing, in the (a) QHS and (b) mirror configurations. The scales are different between the two plots to demonstrate the similar radial extent and frequency range of the bicoherence. The unbiased times produced insignificant bicoherence relative to the noise level.

configuration was not able to measure as far inward as the QHS scan because of a loss of density control with the probe that far in. Nevertheless, the lower level of measured bicoherence with smaller applied E_r is still evident at the innermost point in both configurations.

The scales of the colour bars in figure 6 are not the same in the two configurations, so that the radial extent of the bicoherence can be seen clearly in both cases. The magnitude of the measured bicoherence is higher in the mirror configuration than in QHS, which could be a result of a larger E_r imposed by the bias. The differences in the measured magnitude of bicoherence between the two configurations are indistinguishable given the changes in the imposed radial electric field that is measured.

3.2. Long-range correlations

On the same radial probe scans, another probe was placed at a fixed radial location $\phi = 150^\circ$ toroidally around the machine, as seen in figure 3. This reference probe is located near the mid-plane of the plasma, close to the same poloidal location as the scanning probe. However, with respect to the magnetic field strength of HSX, this reference probe is located at the high-field side of the machine, whereas the 5-pin scanning probe is positioned at the low-field side. Both probes are on the outboard side of the device.

Zonal flows are expected to be a zero frequency mode resulting in a radially sheared flow, and a small perturbation

to the radial electric field. The mode, however, has a finite spectral width, δf , determined by collisional damping [26]. By examining the cross-phase and coherence of low-frequency potential fluctuations at spatially separated points in the plasma, one can look for evidence of the $n = 0$, radially localized zonal flows through this finite-frequency component of the mode. This measurement using multiple probes to analyse the modes is significantly more accessible than direct measurements of the radial electric field or flows with the time resolution necessary to differentiate from the equilibrium values.

To resolve the low-frequency fluctuations, the number of realizations used here had to be smaller than in the bicoherence analysis. Ten realizations were used for the biased times and 20 for the data before the bias was applied. Changes to this frequency resolution/realization balance do not significantly alter the results.

Indications of these long-range correlations are found during biasing in HSX, as presented in figure 7 for both the (a) QHS and (b) mirror configurations. When the bias is applied, the cross-phase between the low-frequency components (< 10 kHz) of the two fluctuating signals goes to zero, and the coherence of the low-frequency fluctuations increases relative to the pre-bias coherence. This is true over roughly the same radial regions in which the induced radial electric field is the strongest, and where the increase in bicoherence is measured. The phase is zero within the statistical uncertainties, the coherence increases relative to the unbiased case, and the coherence is at least 0.6 during biasing for the regions where $0.83 < \rho < 0.93$ in QHS and $0.84 < \rho < 0.95$ in mirror. The noise level for this coherence during the 10 ms of biased time is around 0.3. There are no low-frequency modes observed in the bias current that might explain these measurements as artefacts of the biasing method, nor are GAM oscillations observed in these discharges.

These long-range correlations are observed in potential fluctuations, but density fluctuations do not demonstrate this same behaviour. These are expected characteristics of zonal flows for sufficiently collisionless plasma, and are a compelling piece of evidence that the bicoherence measured is indeed related to zonal flow activity. This is again consistent with previous results from TJ-II in both biased and spontaneous confinement transitions [15], as well as the small stellarator TJ-K. TJ-K has measured long-range correlations in density fluctuations as well as potential during biasing, but this has been attributed to either background density fluctuations or a turbulent drive of zonal density resulting from its high collisionality [16].

4. Conclusions

Measurements of HSX plasmas with multiple Langmuir probe tips have been presented. When a positive bias voltage is applied using a bias probe, a positive radial electric field and corresponding $E \times B$ flow is imposed on the edge of the plasma. In the region of the strongest imposed radial electric field, there is significant auto-bicoherence measured in the fluctuating E_θ signals while the bias is applied. This bicoherence is measured over a broad range of frequencies, and does not display the direct coupling to near-zero frequency zonal flows that has

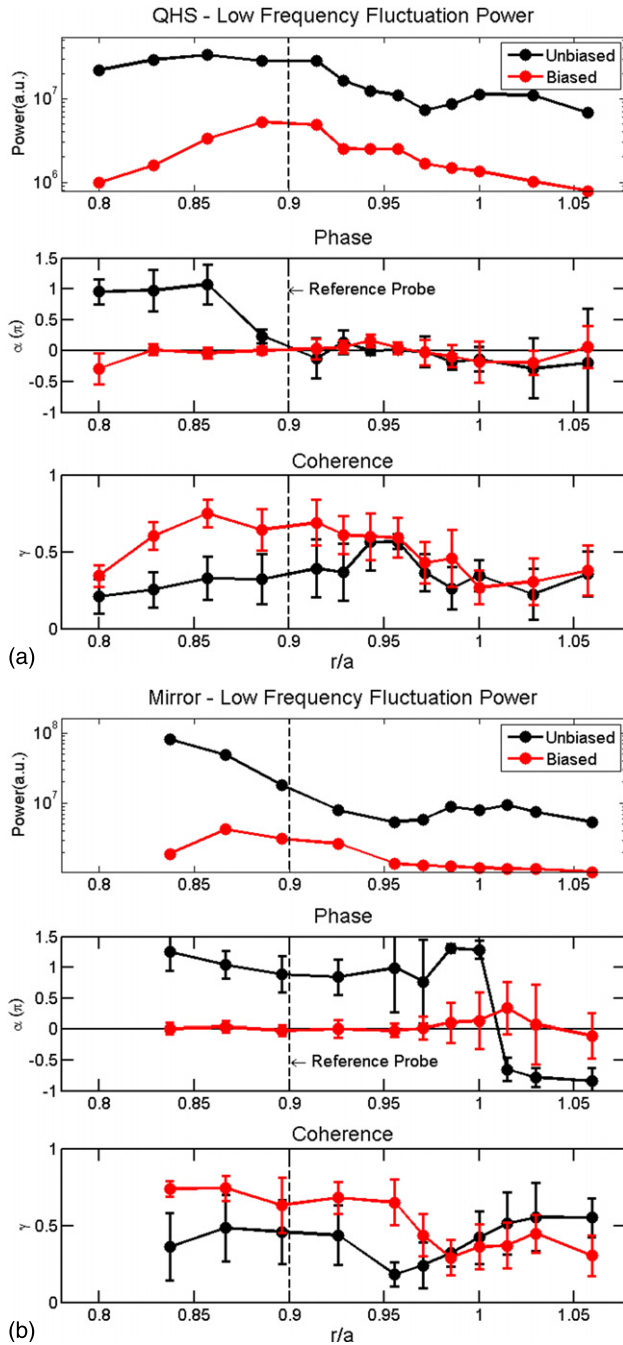


Figure 7. Long-range correlations of low-frequency fluctuations between a scanning probe potential and a stationary reference probe on the far side of the machine in the (a) QHS and (b) mirror configurations. All values are for fluctuations <10 kHz. The radial location of the fixed reference probe is indicated by a dotted line. Phase wrapping was used to smooth the phase plots, which leads to values slightly higher than π in some cases.

been observed during spontaneous confinement transitions in other devices.

These observations reproduce results from TJ-II [7] for biased discharges in three respects. First, the quantity producing the clearest bicoherence is the poloidal electric field. The radial electric field and the radial/poloidal electric field combination do not produce clear bicoherence results. One possible explanation for this observation is that the E_r

scale length is significantly smaller than the E_θ scale length, rendering our method of measurement inadequate. Another explanation may be that the Reynolds stress is not the driving force of the phenomenon being observed.

Second, the bicoherence of the poloidal electric field shows a very clear response to the applied biasing. The level of bicoherence measured before biasing is near the noise level, and when a bias is applied, the bicoherence found is significantly higher than what would be expected for noise. This increased bicoherence is limited to a specific radial range, which corresponds to the region of strong radial electric field and the possible region of zonal flows.

Third, long-range correlations in low-frequency potential fluctuations have been detected during biasing in the same region of large radial electric field. The phase difference between low-frequency potential fluctuations at two spatially separated probes goes to zero, and the coherence increases significantly during the biased times relative to the unbiased times. This is another piece of evidence pointing towards zonal flows as the origin of the broadband bicoherence measurements.

Overall, these measurements show that there is a link between an applied radial electric field, bicoherence and long-range correlations of potential fluctuations below 10 kHz. The general characteristics of these measurements are consistent with steady-state radial electric fields interacting with zonal flows. However, the frequency-resolved bicoherence in HSX shows broadband coupling, very similar to what was observed in biasing experiments at TJ-II, which is distinct from the direct coupling to near-zero frequency zonal flows seen in spontaneous (non-biasing) transitions at several other devices.

There is a slight change in magnitude between the measured bicoherence between the QHS and mirror configurations, but this can be accounted for by the change in imposed radial electric field between the different experiments. Both the level of edge bicoherence and long-range correlations are similar, within experimental error bars, between the mirror and quasi-symmetric configurations.

The main difference between the QHS and mirror configurations is the degree of effective ripple, which determines the deviation of particle orbits from the flux surfaces at zero electric field. Upon applying a radial electric field, this deviation is reduced, and thus the associated difference between the two configurations decreases. It may be, therefore, that the strength of the radial electric field applied in these experiments overwhelms any configurational effect, thus possibly explaining the observed absence of significant differences between configurations.

Acknowledgments

The authors would like to thank Chris Clark, Chuanbao Deng, Mike Frankowski, Konstantin Likin, Paul Probert and Kan Zhai for their assistance throughout the course of this work.

This work was supported in part by the US Department of Energy under Contract No DE-FG02-93ER54222, and by the DGICYT (Dirección General de Investigaciones Científicas y Tecnológicas) of Spain under Project No ENE2009-07247.

References

- [1] Diamond P.H. and Kim Y.-B. 1991 Theory of mean poloidal flow generation by turbulence *Phys. Fluids B* **3** 1626
- [2] Carreras B.A., Newman D., Diamond P.H. and Liang Y.-M. 1994 Dynamics of low to high ('L' to 'H') confinement bifurcation: poloidal flow and ion pressure gradient evolution *Phys. Plasmas* **1** 4014
- [3] Diamond P.H. *et al* 2000 In search of the elusive zonal flow using cross-bicoherence analysis *Phys. Rev. Lett.* **84** 4842
- [4] Ritz C.P., Powers E.J. and Bengtson R.D. 1989 Experimental measurement of three-wave coupling and energy cascading *Phys. Fluids B* **1** 153
- [5] Tynan G.R., Moyer R.A., Burin M.J. and Holland C. 2001 On the nonlinear turbulent dynamics of shear-flow decorrelation and zonal flow generation *Phys. Plasmas* **8** 2691
- [6] van Milligen B.P., Sanchez E., Estrada T., Hidalgo C. and Branas B. 1995 Wavelet bicoherence: a new turbulence analysis tool *Phys. Plasmas* **2** 3017
- [7] van Milligen B.P., Kalhoff T., Pedrosa M.A. and Hidalgo C. 2008 Bicoherence during confinement transitions in the TJ-II stellarator *Nucl. Fusion* **48** 115003
- [8] Watanabe T.-H., Sugama H. and Ferrando-Margalet S. 2008 Reduction of turbulent transport with zonal flows enhanced in helical systems *Phys. Rev. Lett.* **100** 195002
- [9] Sugama H. and Watanabe T.-H. 2005 Dynamics of zonal flows in helical systems *Phys. Rev. Lett.* **94** 115001
- [10] Mynick H.E. and Boozer A.H. 2007 Zonal flows in toroidal systems *Phys. Plasmas* **14** 072507
- [11] Nührenburg J. and Zille R. 1988 Quasi-helically symmetric toroidal stellarators *Phys. Lett. A* **129** 113
- [12] Anderson F.S.B., Almagri A.F., Anderson D.T., Matthews P., Talmadge J.N. and Shohet J.L. 1995 The Helically Symmetric Experiment, (HSX) goals, design and status *Fusion Technol.* **27** 273
- [13] Canik J., Anderson D., Anderson F., Likin K., Talmadge J. and Zhai K. 2007 Experimental demonstration of improved neoclassical transport with quasihelical symmetry *Phys. Rev. Lett.* **98** 085002
- [14] Gerhardt S., Talmadge J., Canik J. and Anderson D. 2005 Experimental evidence of reduced plasma flow damping with quasisymmetry *Phys. Rev. Lett.* **94** 015002
- [15] Pedrosa M., Silva C., Hidalgo C., Carreras B., Orozco R., Carralero D. and TJ-II team 2008 Evidence of long-distance correlation of fluctuations during edge transitions to improved-confinement regimes in the TJ-II Stellarator *Phys. Rev. Lett.* **100** 215003
- [16] Manz P., Ramisch M. and Stroth U. 2009 Poloidal mode structure of long-distance correlation of fluctuations under strong $E \times B$ shear in the torsatron TJ-K *Phys. Plasmas* **16** 042309
- [17] Xu Y. *et al* 2009 Long-distance correlation and zonal flow structures induced by mean $E \times B$ shear flows in the biasing H-mode at TEXTOR *Phys. Plasmas* **16** 110704
- [18] Canik J.M., Anderson D.T., Anderson F.S.B., Clark C., Likin K.M., Talmadge J.N. and Zhai K. 2007 Reduced particle and heat transport with quasisymmetry in the Helically Symmetric Experiment *Phys. Plasmas* **14** 056107
- [19] Nemov V.V., Kasilov S.V., Kernbichler W. and Heyn M.F. 1999 Evaluation of $1/\nu$ neoclassical transport in stellarators *Phys. Plasmas* **6** 4622
- [20] Song D. and Canik J., ORNL 2010 private communication
- [21] Seiwald B., Kasilov S.V., Kernbichler W., Kalyuzhnyj V.N., Nemov V.V., Tribaldos V. and Jiménez J.A. 2008 Optimization of energy confinement in the $1/[n]$ regime for stellarators *J. Comput. Phys.* **227** 6165
- [22] Mahdizadeh N., Greiner F., Ramisch M., Stroth U., Guttenfelder W., Lechte C. and Rahbarnia K. 2005 Comparison of Langmuir and emissive probes as diagnostics for turbulence studies in the low-temperature plasma of the torsatron TJ-K *Plasma Phys. Control. Fusion* **47** 569
- [23] Guttenfelder W., Lore J., Anderson D., Anderson F., Canik J., Dorland W., Likin K. and Talmadge J. 2008 Effect of quasihelical symmetry on trapped-electron mode transport in the HSX Stellarator *Phys. Rev. Lett.* **101** 215002
- [24] Moyer R., Tynan G., Holland C. and Burin M. 2001 Increased nonlinear coupling between turbulence and low-frequency fluctuations at the L-H transition *Phys. Rev. Lett.* **87** 135001
- [25] Nagashima Y. *et al* 2006 Bispectral analysis applied to coherent floating potential fluctuations obtained in the edge plasmas on JFT-2M *Plasma Phys. Control. Fusion* **48** S1
- [26] Hahm T.S., Burrell K.H., Lin Z., Nazikian R. and Synakowski E.J. 2000 Zonal flow measurements concept I *Plasma Phys. Control. Fusion* **42** A205